Germanium Adsorption and Initial Growth on SrTiO3 (001) Surface: A First-Principles Investigation

ARTICLE *in* THE JOURNAL OF PHYSICAL CHEMISTRY C · OCTOBER 2011

Impact Factor: 4.77 · DOI: 10.1021/jp205074w

2 AUTHORS:

Junjie Wang
National Institute for Materials Science
17 PUBLICATIONS **152** CITATIONS
SEE PROFILE

Isabelle Lefebvre
Institut Supérieur de l'Electronique et du Nu…
42 PUBLICATIONS **622** CITATIONS
SEE PROFILE

THE JOURNAL OF PHYSICAL CHEMISTRY C

ARTICLE

pubs.acs.org/JPCC

Germanium Adsorption and Initial Growth on $SrTiO_3$ (001) Surface: A First-Principles Investigation

Junjie Wang* and Isabelle Lefebvre

IEMN, Departement ISEN (UMR 8520 CNRS), 41 boulevard Vauban, 59046 Lille Cedex, France

ABSTRACT: The initial stages of germanium (Ge) adsorption and heteroepitaxial growth on the $SrTiO_3$ (001) surface have been investigated with first-principles calculations. Our results reveal that the 2 × 1 DL TiO_2 reconstruction plays a major role in the Ge chemisorption. This surface reconstruction involves a charge transfer between Ti and O atoms at the surface that locally increases the attractiveness for Ge nucleation. The calculated charge transfer is in good agreement with the core level shift observed by soft X-ray photoemission spectroscopy. Moreover, our potential-energy surface calculations for Ge adatoms on the $SrTiO_3$ (001) 2 × 1 DL TiO_2 surface show that the surface diffusions of Ge atoms are highly anisotropic. Ge adatoms are easy to jump from other sites to the most stable site nearby the floating oxygen with energy barriers <0.45 eV. Therefore, the Ge adsorption configuration around surface floating oxygen atom, a particularity of this surface, is identified as the nucleation center of the further Ge (111) growth. A route for a bidimensional (111)-oriented growth of Ge on STO(001) surface has been identified and confirmed by the X-ray photoemission spectroscopy experiment results. These findings help us to understand how the 2 × 1 DL TiO_2 reconstruction can be the starting point for the growth of (111)-oriented Ge on STO(001).

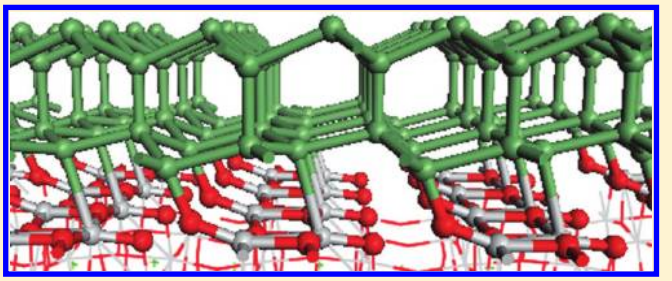

1. INTRODUCTION

Germanium is one of the most promising high mobility semiconductors to replace Si in high-speed complementary metal-oxide-semiconductor (CMOS) circuits. Integrating Ge semiconductor on Si substrate can allow designing high-performance systems combining opto- and microelectronic functionalities on the low-cost Si platform. However, the development of Ge-based semiconductors application is impeded because of difficulties in the defect-free heteroepitaxial Ge growth on Si. The direct growth of Ge on silicon is made difficult by the too-large lattice mismatch between the materials.

Recently, several groups[1−4] have proposed growing epitaxial oxides on Si as buffer layer to accommodate the lattice mismatch between Ge and substrate. In particular, Saint-Girons et al. have studied the crystalline growth of Ge and III−V semiconductors on various oxide/Si crystalline buffers, for example, Gd_2O_3/Si (111),[5] $LaAlO_3$(LAO)/Si(001),[6] and $SrTiO_3$(STO)/Si(001).[7,8] Although there are many kinds of candidate buffer layer oxides, STO can be directly grown on Si(001) and presents good structural quality, that is, single crystalline and domain growth, low defect density, and rms <0.3. Therefore, STO could be regarded as an excellent potential buffer layer to accommodate the Si−Ge lattice mismatch.

At INL (Institut des Nanotechnologies de Lyon), our colleagues have carried out some studies of the InP growth on both STO(001) and STO/Si(001) templates and found that the surface reconstruction has an important influence on the growth of InP.[9] They also studied the growth of Ge on STO-(001) surfaces.[10] Solid source molecular beam epitaxy (MBE) experiments have shown that an actual Ge layer-by-layer growth on STO (001) surface is possible. However, the STO surface must be activated via annealing to favor Ge chemisorption. As a result, the initial surface reconstruction could be of prime importance for selecting between the two possible growth orientations, namely, Ge (001) and (111). These two orientations have been identified by reflection high-energy electron diffraction (RHEED) during the growth for similar growth conditions.

Consequently, a precise control of the monolayer growth of Ge on STO surface requires detailed knowledge of the initial reactions of Ge atom with STO surfaces on atomic scale. Many experimental and theoretical works have been done to study unreconstructed[11−14] and reconstructed[15,16] STO (001) surface; however, the initial Ge adsorption processes even at submonolayer coverage are not yet fully understood, especially on STO (001) surfaces. Depending on the experimental environment, STO(001) surfaces can undergo many structural transformations, from various reconstructions to the formation of nanostructures on the surface. Among these surface reconstructions, STO(001) 2 × 1 double-layered (DL) TiO_2 (labeled as STO-(001) in the following context) surface has been proved as a stable surface structure in experimental[15] and theoretical.[16] Therefore, this reconstruction will be our starting point for the following.

Received: May 31, 2011
Revised: October 3, 2011

   dx.doi.org/10.1021/jp205074w | J. Phys. Chem. C XXXX, XXX, 000–000

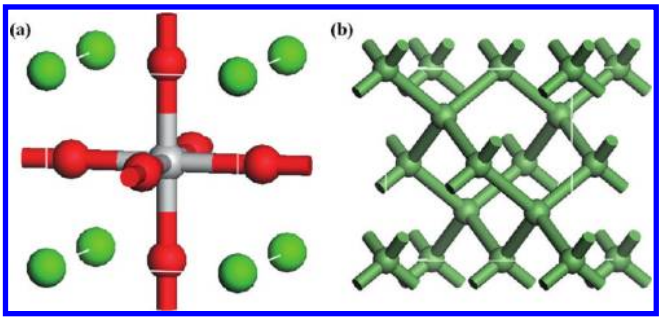

Figure 1. Bulk structures of $SrTiO_3$ (a) and Ge (b). In this and all following figures related to the surface structure, green, gray, red, and olive spheres, respectively, indicate Sr, Ti, O, and Ge atoms.

Table 1. Experimental and Calculated Lattice Parameters of STO and Ge

		a (Å)	*B* (GPa)	C44 (GPa)	B/C44
STO	exptl[17]	3.90	174	124	1.41
	calcd (GGA-PBE)	3.94	172	110	1.56
Ge	exptl[18]	5.65	77	68	1.13
	calcd (GGA-PBE)	5.66	77	67	1.15

In this Article, therefore, we examine the relative stability of the adsorption sites, the interaction between adsorbed Ge atoms, and the formation of initial Ge tetrahedral structure on the STO(001) surface. This allows us to define the most probable interface of the Ge epitaxy initial stage. Finally, some insights about the spontaneous Ge growth orientation on STO(001) surface will be drawn. These first-principles calculation results will be confronted to soft-X-ray photoemission experiments.

The Article is organized as follows. In Section 2, we briefly describe the model of STO(001) surface and address the calculation method. In Section 3.1, we report our results on the STO(001) surface relaxation. In Sections 3.2 and 3.3, the adsorptions of single Ge atom and Ge atom pairs on STO(001) surface are, respectively, studied. In Section 3.4, a possible formation process of first Ge (111) tetrahedral structure on STO(001) surface has been proposed. A short summary is given in Section 4.

2. MODEL BUILDING AND CALCULATION FRAMEWORK

The space groups of STO and Ge are $Pm\bar{3}m$ and $Fd\bar{3}m$ (Figure 1), respectively. Experimental lattice parameters for bulk STO and Ge are given in Table 1. Because of the difference of these two structures, the epitaxy of Ge on STO cannot be realized in the classical "cube-on-cube" scheme.

In the present study, geometries of STO bulk and surface structure were fully optimized using the ultrasoft plane-wave pseudopotential density functional method within the generalized gradient approximation (GGA) frameworks as implemented in CASTEP.[19] The GGA functional provided in CASTEP and adopted here is the Perdew–Burke–Ernzerhof (PBE)[20] version. The convergence criteria for energy, force, and displacement of bulk optimizations are, respectively, 5×10^{-6} eV/atom, 0.01 eV/Å, and 5×10^{-4} Å. We employ a Monkhorst-Pack[21] sampling scheme with a k-point mesh of $6 \times 6 \times 6$ for STO and Ge bulks. The plane wave basis set was restricted by a cutoff energy of 380 eV.

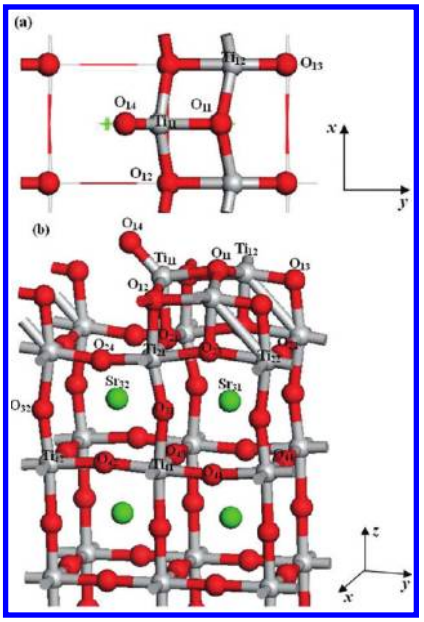

Figure 2. Top (a) and side (b) views of relaxed STO(001) surface structure.

The calculated parameters of STO and Ge are presented in Table 1. The good agreement between experimental values and our computed values shows the quality of the theoretical description.

A periodically repeated 11-layer-thick 2×1 slab-supercell, which is separated from its *z*-direction neighbors by a 20 Å vacuum width, was used in modeling the STO surfaces. Tests with larger model sizes have shown that present model setting is sufficient.

In the slab model surface relaxation and germanium atom adsorption calculations, the computational parameters were different from the bulk lattice parameter computations because of larger computational requirements. Here the convergence criteria for energy, force, and displacement are, respectively, 5×10^{-5} eV/atom, 0.1 eV/Å, and 5×10^{-3} Å. A Monkhorst-Pack[3] sampling scheme with a k-point mesh of $5 \times 3 \times 1$ for surface structure is employed. The plane-wave basis set was restricted by a cutoff energy of 380 eV.

The adsorption energies can be calculated using the following equation

$$\Delta E_{ads} = \frac{N \cdot E_{Ge} + E_{slab} - E_{total}}{N} \quad (1)$$

where N is the number of Ge atoms adsorbed on the STO surface. E_{slab}, E_{Ge}, and E_{total} denote the calculated total energies per supercell calculated for the clean STO slab, isolated Ge atom, and the slab with Ge adsorbed on the surface, respectively. ΔE_{ads} is positive if the adsorption of atomic Ge on the surface is favorable and exothermic.

3. RESULTS

In this section, we present the optimized structures of a variety of Ge-adsorbed STO(001) surfaces as resulting from our calculations for different Ge adatoms. For convenience, we label a lattice structure with X_{ij} atoms on the additive, first, second, and third layers (as illustrated in Figure 2), where X represents Ti, O, and

dx.doi.org/10.1021/jp205074w |J. Phys. Chem. C XXXX, XXX, 000–000

Table 2. Atomic Displacement in y and z Directions Calculated in Present Study (In Percent of Bulk Lattice Constant) for STO (001) 2 × 1 DL TiO_2 Surface Are Compared with Those Obtain in Heifets and Erdman's Works

		Δx	Δy			Δz		
layer	atom	present	present	ref 16	ref 15	present	ref 16	ref 15
+I	Ti_{11}	0.42	−5.11	−5.84	−7.04	15.50	14.73	15.70
	Ti_{12}	1.71	4.61	4.28	4.10	8.59	6.09	10.19
	O_{11}	0.11	−4.82	−5.58	−5.84	21.26	19.16	23.61
	O_{12}	0.38	0.69	0.14	0.58	4.91	2.79	5.89
	O_{13}	−0.23	−0.99	−1.26	−0.92	3.19	1.29	4.30
	O_{14}	0.18	20.41	22.77	14.04	48.14	49.93	45.89
I	Ti_{21}	−0.85	−3.76	−3.13	−2.92	3.07	1.05	3.41
	Ti_{22}	−3.67	2.77	3.19	2.80	5.41	2.97	5.99
	O_{21}	0.61	−3.79	−3.34	−4.58	8.61	5.80	10.19
	O_{22}	1.19	0.67	1.02	0.46	−0.42	−2.88	−0.69
	O_{23}	1.37	0.29	0.24	−0.14	11.57	8.83	12.01
	O_{24}	0.65	−0.17	0.24	0.02	−3.13	−4.71	−3.20
II	Sr_{31}	−0.80	−0.36	1.42	1.84	7.78	3.73	5.51
	Sr_{32}	−0.65	−3.08	−1.61	−1.94	3.35	1.22	3.51
	O_{31}	0.13	6.02	4.99	6.18	6.73	3.80	6.30
	O_{32}	0.56	−4.80	−3.74	−5.00	2.69	1.02	2.89
III	Ti_{41}	−0.53	−1.27	0.21	0.42	2.52	1.58	3.00
	Ti_{42}	−0.34	−2.85	−0.99	−0.46	4.06	2.39	4.20
	O_{41}	0.32	0.10	−0.11	−0.18	0.00	0.00	0.00
	O_{42}	0.20	1.27	0.86	0.30	6.85	3.93	7.09
	O_{43}	0.28	1.19	0.27	0.00	5.31	2.74	4.99
	O_{44}	0.25	0.86	0.58	0.10	2.21	1.40	2.61

Sr atoms, i equals 1, 2, 3, and 4 for additive, first, second, and third layers, respectively, and j labels the sequence of X atom in certain layer.

3.1. STO(001) Surface Relaxation. The optimally relaxed structure and data in comparison with those of unrelaxed surfaces for STO(001) surface cell are, respectively, illustrated and shown in Figure 2 and Table 2. In the relaxation, the topmost four layers were relaxed along x, y, and z directions. Atomic displacements along the y and z directions for STO(001) surface calculated in this study were compared with those obtained in refs 15 and 16 (Table 2). Our equilibrium geometries for this reconstruction are in good agreement with former investigations. However, there is a difference between our study and former calculations: that is, the atoms were not allowed to relax along the x direction in Heifets et al.'s calculations.[16] Our calculation result shows that the surface symmetry along z axis is still kept with a very little atomic displacements along the x direction after the surface relaxation.

The calculated Bader charges[22] and Mulliken bond populations of bulk $SrTiO_3$ are reported in Table 3. Bader charge analysis is a kind of approach proposed by Bader[23] to obtain the partial atomic charges in molecules based solely on the charge density distributions. Compared with the orbital-based Mulliken analysis, Bader charge analysis is basis set independent and has been extensively used in recent years. Present calculations are carried out with plane wave basis functions, which are not associated with any particular atom in the system;[22] therefore, Mulliken analysis is not applicable for the partial atomic charge analysis. However, the Mulliken bonding population analysis is still a useful tool for describing covalency of bonding and bond strength.[24] Consequently, Bader charge and Mulliken bonding population analysis are both used in the present study. Table 3 shows that because of the little covalent content of the Sr−O bond (P_{Sr-O} = 0.10|e|), charge of the Sr atom (1.60|e|) is relatively close to its formal charge (2|e|). On the contrary, charge of Ti(2.17|e|) atom is far from its +4|e| formal charges because of the covalent nature of Ti−O bond (P_{Ti-O} = 0.90|e|). The charge of O (−1.26|e|) atom is moderate comparing its −2|e| formal charge due to the compromising covalence of Ti−O and Sr−O bondings. Our calculation results and those obtained in ref 25 are in good agreement.

Table 3. Calculated Partial Atomic Charges and Bond Populations in |e| for Bulk STO

		ion			bond	
		O	Ti	Sr	Ti−O	Sr−O
atomic charge	present	−1.26	2.17	1.60		
	ref 25	−1.28	2.24	1.60		
bond population	present				0.90	0.11

Table 4. Calculated Partial Atomic Charges Q in |e| and Their Deviations from Bulk Values Q_{bulk} (listed in Table 3) for the Outermost Layers of STO(001) Surface

		ref 16		present	
layer	atom	Q	ΔQ_{bulk}	Q	ΔQ_{bulk}
+I	Ti_{11}	2.16	−0.19	2.02	−0.15
	Ti_{12}	2.26	−0.10	2.10	−0.07
	O_{11}	−1.26	0.15	−1.17	0.09
	O_{12}	−1.38	0.03	−1.22	0.04
	O_{13}	−0.96	0.45	−0.93	0.33
	O_{14}	−0.77	0.64	−0.80	0.46
I	Ti_{21}	2.32	−0.04	2.15	−0.02
	Ti_{22}	2.31	−0.05	2.17	0.00
	O_{21}	−1.35	0.06	−1.22	0.04
	O_{22}	−1.29	0.12	−1.18	0.08
	O_{23}	−1.26	0.15	−1.15	0.11
	O_{24}	−1.22	0.19	−1.15	0.11
II	Sr_{31}	1.86	−0.01	1.61	0.01
	Sr_{32}	1.86	−0.01	1.60	0.00
	O_{31}	−1.40	0.01	−1.25	0.01
	O_{32}	−1.41	−0.01	−1.24	0.02
III	Ti_{41}	2.35	0.00	2.15	−0.02
	Ti_{42}	2.35	0.00	2.16	−0.01
	O_{41}	−1.37	0.04	−1.22	0.04
	O_{42}	−1.43	−0.02	−1.25	0.01
	O_{43}	−1.40	0.01	−1.24	0.02
	O_{44}	−1.41	0.00	−1.26	−0.00

The Bader partial atomic charges and their deviations from the bulk values for STO(001) surface are calculated and listed in Table 4. As observed in former research,[15,16,26] our calculation results show that the charges of surface atoms decreased, especially for the surface Ti atoms and O_{13} and O_{14} (surface floating oxygen) oxygen atoms. This means that negative charges are transferred from O atoms to Ti atoms on the STO(001)

dx.doi.org/10.1021/jp205074w |J. Phys. Chem. C XXXX, XXX, 000–000

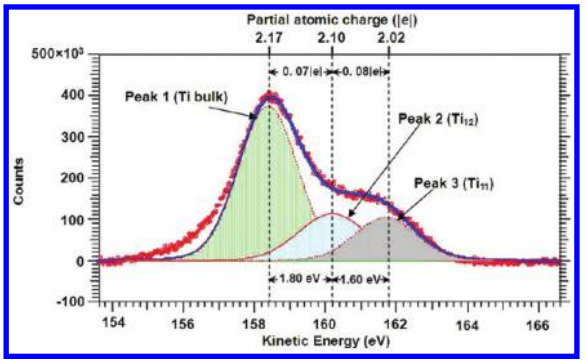

Figure 3. Ti 3p core level for annealed STO(001) surface[10] recorded at $h\nu$ = 200 eV at TEMPO beamline (Soleil).

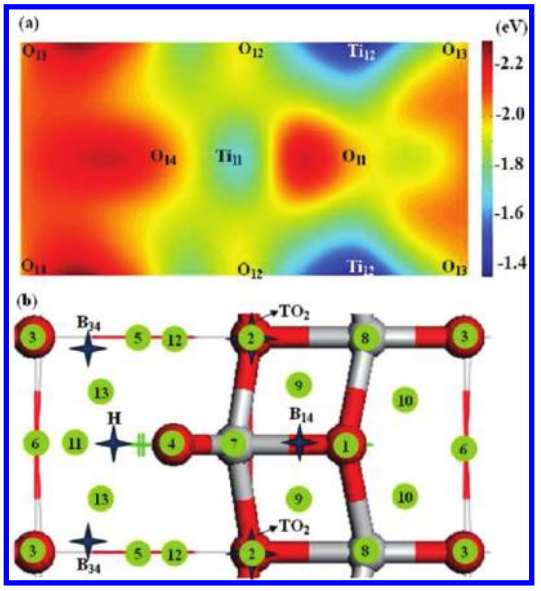

Figure 4. Potential energy surface of Ge adsorption (a) and possible Ge adsorption sites (b) on STO(001) surface. Green circles and blue stars in panel b, respectively, illustrate the initial and final Ge adsorption sites.

surface. However, the difference between the gain of Ti atoms and loss of O atoms suggests that the covalent content of Ti−O bondings is also increased. The partial charges listed in Table 4 show that the Ti atoms can be classified into three groups: Ti-bulk (2.17|e|), Ti_{12} (2.10|e|), and Ti_{11} (2.02|e|).

This result is in good agreement with the experimental results from ref 10. In this experiment, $SrTiO_3$ was annealed to 900 °C (to activate the surface) and recorded using soft X-ray synchrotron radiation photoemission. Figure 3 shows a typical Ti 3p core level spectrum recorded at $h\nu$ = 200 eV. This spectrum has been decomposed into three components: peak 1 with a binding energy at 41.6 eV, which clearly corresponds to bulk Ti atoms, and peaks 2 and 3 at 39.8 and 38.2 eV, which are related to two different TiOx oxidation states. As already done in refs 27. and 28, one may consider that photoemission core level shifts are roughly proportional to charge transfers. In other words, the Ti surface atoms are less positively charged and thus the related photoemission peaks appear at lower binding energy than that of bulk-Ti-related peaks. This charge transfer on the surface also means that the surface O atoms, especial O_{13} and O_{14} (surface floating oxygen), will be "charge deficient" and easier to adsorb Ge atoms in the Ge growth process.

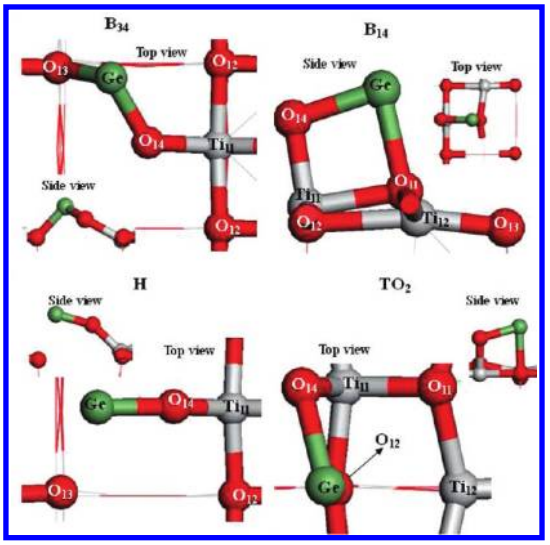

Figure 5. Top and side views of the optimized possible Ge atom adsorption sites on the STO(001) surface.

Table 5. Adsorption Energies and Evolutions of Ge Atom Adsorption on the STO(001) Surface

final configuration	initial configuration	adsorption energy (eV/atom)
B_{34}	3, 5, 6, 10, 11, 12, and 13	4.45
B_{14}	1, 7, 8, and 9	3.79
H	4	3.73
TO_2	2	3.12

3.2. Single Ge Atom Adsorption on STO(001) Surface. By optimizing the Ge atom positions along z direction on different adsorption sites, a series of minimum energies are obtained and used to get a 2D Ge adsorption energy surface (see Figure 4a) on STO (001) 2 × 1 DL TiO_2 surface cell. The energy surface map shows that all of the energy minimums are adjacent to surface O atoms. This reveals that the surface O atoms will be more active than surface Ti atoms in the Ge atom adsorption process.

To estimate the influence of surface relaxation on the Ge adsorption, we carried out a series of quasi-static calculations. Thirteen possible adsorption sites (illustrated in Figure 4b) are considered in the present work. After geometry optimization, four stable adsorption sites on the STO(001) surface are obtained (shown in Figure 4b and Figure 5). The calculated adsorption energies, evolutions for these adsorption sites, and structural parameters for these adsorption sites are listed in Tables 5 and 6.

Figure 5 shows four different Ge adsorption stable configurations, which can be divided into three groups: "bridge" sites between two O atoms(B_{14} and B_{34}), "on top" site (TO_2), and "hollow" site (H). From the adsorption energies listed in Table 5, the chemisorption of Ge atom was found to be strongly exothermic, and the Ge adsorption at B_{34} site produces the configuration with lowest energy. It is clearly seen from Figure 4 that the four stable adsorption positions are all located at the energy minimal zones of the potential energy surface. This reflects the fact that STO surface structure has a dominant influence on the single Ge atom adsorption.

dx.doi.org/10.1021/jp205074w |J. Phys. Chem. C XXXX, XXX, 000–000

Table 6. Detailed Bond Parameters of Stable Adsorption Structures of Single Ge Atom on STO(001) Surface

configuration	bond	distance (Å)	population (|e|)
B_{34}	Ge−O_{13}	1.90	0.33
	Ge−O_{14}	1.87	0.43
B_{14}	Ge−O_{11}	2.10	0.13
	Ge−O_{14}	1.80	0.33
H	Ge−O_{14}	1.80	0.41
TO_2	Ge−O_{12}	2.21	0.14
	Ge−O_{14}	2.02	0.29

Table 7. Energy Barriers for Germanium Atom Diffusion between Adsorption Sites on STO(001) Surface

initial position	final position	energy barrier (eV)
H	B_{14}	0.36
H	B_{34}	0
H	TO_2	0.39
B_{14}	B_{34}	0.76
B_{14}	TO_2	0.96
B_{14}	H	0.45
B_{34}	B_{14}	1.33
B_{34}	TO_2	1.36
B_{34}	H	0.82
TO_2	B_{14}	0.29
TO_2	B_{34}	0.03
TO_2	H	0.02

The data listed in Table 6 also show that the Ge−O bonds of the B_{34} configuration (Figure 5) are the strongest because of largest bond populations and short bond lengths. By combining of the adsorption energy results and adsorption configuration structure parameters, we can confirm that B_{34} is the most stable single Ge atom adsorption configuration.

The diffusions of Ge atom on the surface are investigated by calculating the energy barriers to be overcome when moving from one stable site to another. The minimum-energy paths (MEPs) connecting the initial and final states of each migration step and energy barriers for Ge atom diffusions are obtained with the complete linear synchronous transit (LST)/quadratic synchronous transit (QST) method approach.[29] The energy barriers listed in Table 7 indicate that the Ge diffusions from TO_2 site to B_{34} and H sites are activated with very low energy cost of about 0.03 and 0.02 eV, respectively, and no energy barrier can be found between H and B_{34} configurations. This result reveals that TO_2 and H configurations are metastable and can be easily translated to B_{34} under a little disturbance, for example, a neighbor Ge adsorbate. The energy barriers for germanium diffusion from TO_2 and H to B_{14} are, respectively, about 0.29 and 0.36 eV, which are one order higher than the diffusion to B_{34}. The diffusion between B_{14} and B_{34} is quiet difficult because of high energy barriers of about 0.76 eV (B_{14} to B_{34}) and 1.33 eV (B_{34} to B_{14}). However, the energy barrier from B_{14} to H is 0.45 and much lower than that from B_{14} to B_{34}, which means that the diffusion from B_{14} to B_{34} can be achieved with a much lower activation energy along the route: $B_{14} \rightarrow H \rightarrow B_{34}$. On the basis of these results, we can show that at the ordinary growth temperatures the deposited Ge atom has a high probability to move from other sites to B_{34}. Therefore, B_{34} configuration has the highest likelihood to act as nucleation center in the following steps.

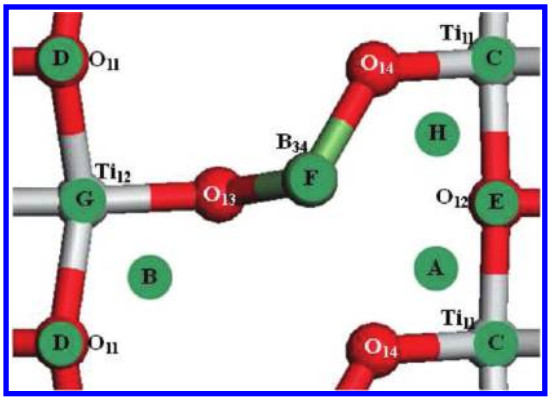

Figure 6. Possible configurations of double Ge atoms adsorption on STO(001) surface. Green circles with capitals illustrate the initial second Ge adorption sites.

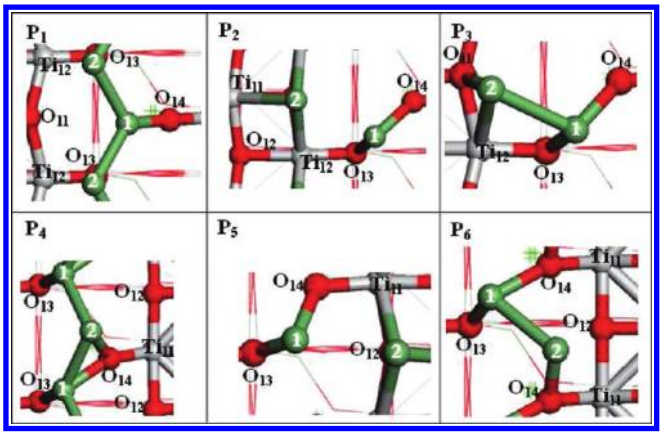

Figure 7. Stable configurations of double Ge atoms adsorption on STO(001) surface. All Ge atoms are labeled with their adding sequence.

Table 8. Adsorption Energies and Evolutions of Ge Atom Pairs Adsorption on the STO(001) Surface

final configuration	initial configuration	adsorption energy (eV/atom)
P_1	B_{34}−F	3.98
P_2	B_{34}−C	3.94
P_3	B_{34}−B and B_{34}−D	3.91
P_4	B_{34}−G	3.87
P_5	B_{34}−E and B_{34}−H	3.76
P_6	B_{34}−A	3.72

3.3. Adsorptions of Ge Atom Pairs on STO(001) Surface. In the Ge growth process, the Ge atoms will adsorb on the STO surface one by one, therefore, adsorption structure and energetics could be different in the presence of a neighboring Ge adatom. Our study indicates that B_{34} is the most stable single Ge atom adsorption configuration on the STO(001) surface and could be regarded as the nucleation center. Hence, we present a systematic investigation in this section to study the second germanium atom adsorption around B_{34} configuration.

By considering the relative positions of Ge atoms, the size of our unit cell and the periodicity condition at boundaries, we have

dx.doi.org/10.1021/jp205074w |J. Phys. Chem. C XXXX, XXX, 000–000

Table 9. Detail Parameters of Optimized Ge(111) Tetrahedral (F) and Ge(111)/STO Interface (I) Structures Are Compared with Ideal Ge Bulk Bond (2.45 Å) and Angle (109.5°), Ti−Ge Bond Length (2.76 Å),[31] and Ge−O Bond Length in Bulk Germania (1.74 Å)[30]

parameter	label	structure	value	error (%)
bond	Ge_1-Ge_2	F	2.52 Å	2.85
		I	2.50 Å	2.04
	Ge_2-Ge_3	F	2.68 Å	9.38
		I	2.67 Å	8.97
	Ge_3-Ge_4	F	2.44 Å	−0.41
		I	2.48 Å	1.22
	Ge_1-Ge_4	F	2.67 Å	8.98
		I	2.66 Å	8.57
	Ge_1-O_{14}	F	1.89 Å	8.62
		I	1.83 Å	5.17
	Ge_3-Ti_{12}	F	2.90 Å	5.07
		I	2.70 Å	−2.17
angle	$\angle Ge_1-Ge_2-Ge_1$	F	102.6°	−6.30
		I	107.8°	−1.55
	$\angle Ge_1-Ge_2-Ge_3$	F	114.5°	4.56
		I	119.6°	9.22
	$\angle Ge_1-Ge_4-Ge_3$	F	119.7°	9.31
		I	110.9°	1.28
	$\angle Ge_3-Ge_4-Ge_3$	F	107.8°	−1.55
		I	105.4°	−3.74

built eight possible combinations of adsorption sites around B_{34} Ge atom, which are illustrated in Figure 6. Starting from the relaxed B_{34} configuration, we added a second Ge atom at a possible site illustrated in Figure 6 and let the model relax. After geometry optimization, six stable configurations (P_1-P_6) were obtained. (See Figure 7.) The detailed structure evolutions and adsorption energies of Ge atom pairs are listed in Table 8.

By studying the evolution of adsorption configurations, we find that most B_{34} involved in these initial configurations remains stable after optimization. This result proves once again that B_{34} configuration is very stable and can preserve its position under the external disturbance. From the energy barrier data listed in Table 8, we know that Ge atom at B_{34} site has the highest probability to move to H site under a large disturbance because of the smaller energy barrier of 0.82 eV. This is proved by the evolution from $B_{34}-F$ to P_1 configuration. Ge_1 atom broke the bond with O_{13} and moved to H site. The bond angles in configuration P_1: $\angle Ge_1-Ge_2-Ge_1$ and $\angle Ge_2-Ge_1-Ge_2$ are both 108.7°, which are very close to the bond angle of 109.5° in the germanium bulk. Consequently, P_1 configuration can be regarded as a transitional structure of Ge initial growth on STO(001) surface. By comparing the values of adsorption energies listed in Table 9, we can show that configuration P_1 is the most stable Ge atom pair adsorption structure. Although the energy difference between configurations is not so important as in the single Ge atom adsorption case, the other configurations than the most stable P_1 seem to be a bad starting point to construct further a Ge (111) plane. Therefore, P_1 could be used as a starting structure to build the first Ge tetrahedral in the next step.

3.4. Formation of First Plane of the Ge (111) Structure. Surrounding the most stable Ge atom pair adsorption configuration

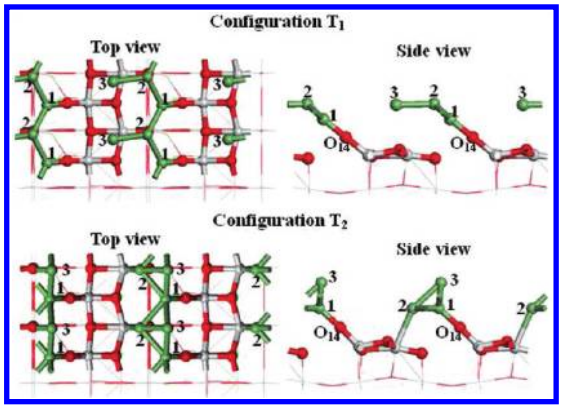

Figure 8. Optimized configurations of triple Ge adsorption on STO-(001) surface. All Ge atoms are labeled with their adding sequence.

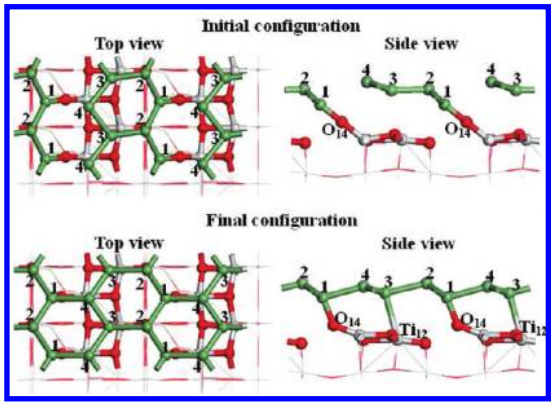

Figure 9. Initial and optimized configurations of Ge tetrahedral structure F_1 on STO(001) surface. All Ge atoms are labeled with their adding sequence.

(P_1) achieved in last section, we supplied further Ge atoms at different sites to investigate the formation of first Ge tetrahedral structure. First, we investigated the adsorption of the third Ge atom by taking into account all possible adsorption sites around P_1. After full relaxation, two stable triple Ge atom adsorption configurations (labeled as T_1 and T_2 in Figure 8) are obtained. The adsorption energies of T_1 and T_2 are, respectively, 3.87 and 4.12 eV/atom. The third Ge atom in configuration T_1 is connected to P1 configuration only through a onefold bond with the second adsorbed Ge, which is unstable regarding the sp^3 bond type character of germanium. On the contrary, a three-fold-coordinated Ge_3 adsorption is obtained in T_2 configuration after geometry optimization. Therefore, T_2 configuration is in a lower energy state and more stable than T_1. By means of the complete LST/QST method, we found the minimum energy path (MEP) connecting T_1 and T_2 configurations and confirmed the energy barriers. The computed values indicate that the transition from T_1 to T_2 is activated with a low energy cost of ~0.56 eV, whereas the energy barrier for transition from T_2 to T_1 (1.22 eV) is about two times higher. This result reveals that the T_2 configuration has a high probability to exist at the lower growth temperatures. In higher temperature conditions, the high energy barrier from T_2 to T_1 can be overcome because of the higher kinetic energy of Ge atoms; therefore, the existence probability of T_1 at higher temperature will also increase.

We therefore continuously proceeded the Ge growth study based on the two different triple Ge adsorption configurations

dx.doi.org/10.1021/jp205074w |J. Phys. Chem. C XXXX, XXX, 000–000

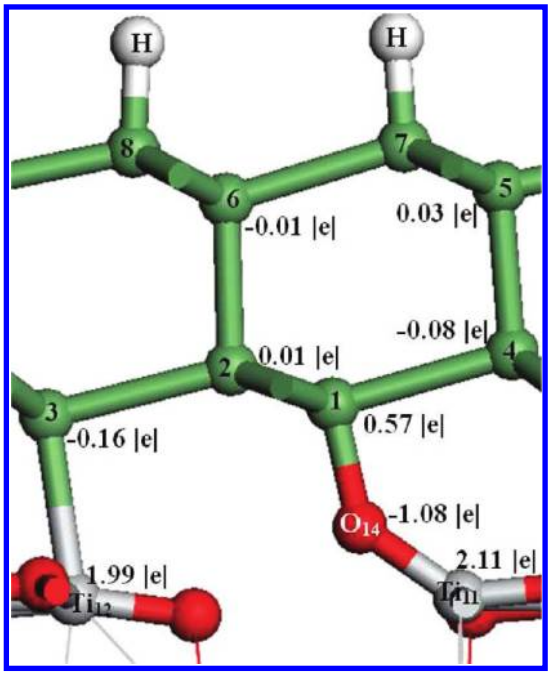

Figure 10. Atomic configuration of the relaxed Ge(111)/STO structure. All Ge atoms are labeled with their adding sequence, and the topmost Ge atoms are saturated with hydrogen atoms.

(T_1 and T_2). Our calculations (not included in present Article) show that the Ge growth from T_2 configuration is very complex and leads to unrealistic structures. Consequently, we present only the study based on the T_1 configuration despite the fact that T_2 is in a lower energy level state.

In T_1 configuration, Ge_3 atom is one-fold-coordinated; therefore, it has the most free electrons to bond the following adsorbed Ge atom. The initial configuration of four Ge atoms adsorption is constructed by putting the fourth Ge atom next to Ge_3 in the surface cell, as illustrated in Figure 9. In this case, after relaxation, a well-organized and stable Ge (111) layer (Labeled as F) is produced on the STO(001) surface. This is consistent with the experiment that (111) is a main Ge growth direction on STO (001) surface. From Figure 9, we can learn that Ge_1, Ge_2, and Ge_4 are located at the three bottom positions of the potential energy density map (see Figure 6a) of STO (001) 2 × 1 DL TiO_2 surface. This result shows that the potential energy distribution of the STO surface has an important influence on the Ge initial growth. The adsorption energy of the first plane of Ge (111) structure is 4.11 eV/atom, which is larger than that of T_1 configuration. The detail structure of this structure is listed in Table 9. This structure is consistent with experimental observation that the [110]Ge direction is parallel to the [100]STO direction. Although there is a little deviation (<10%) from the ideal Ge bulk structure, this configuration can be regarded as a good foundation for a Ge [111] direction growth.

On the basis of the Ge tetrahedral structure shown in Figure 9, we built a Ge(111)/STO interface structure consisting of STO (001) surface and a slab of four germanium layers whose topmost layer is passivated with hydrogen atoms. The detail parameters and atomic configuration of the relaxed Ge(111)/STO structure (Labeled as I) are, respectively, listed and illustrated in Table 9 and Figure 10. Smaller deviations of Ge bond lengths and angles from Ge bulk are observed after relaxation compared with configuration F. By regarding their partial atomic charges

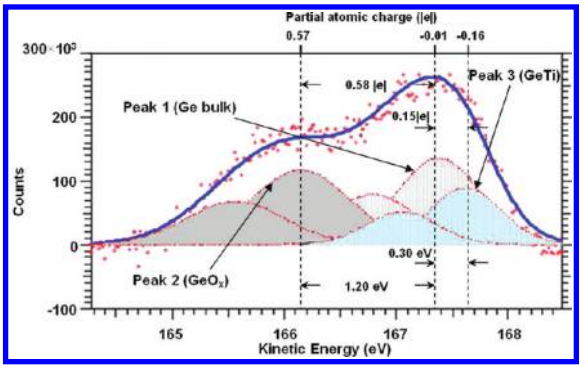

Figure 11. Ge 3d core level for Ge on an annealed STO(001) surface recorded at $h\nu$ = 200 eV at TEMPO beamline (Soleil).[10]

(shown in Figure 10), the Ge atoms (not include Ge_7 and Ge_8) in the configuration I can be classified into three groups: (1) bulk Ge (Ge_2, Ge_4, Ge_5, and Ge_6, −0.01|e| of average charge) tightly bound neighboring Ge atoms with typical sp_3 bondings; (2) oxidized Ge (Ge_1) bonding with surface oxygen atom (0.57|e|); and (3) GeTi (Ge_3, −0.16|e|) bonding with surface Ti_{12}. The computed Ge−O bond length decreases from 1.89 Å in configuration F to 1.83 Å in configuration I. We note that the later value is 5.17% larger than the experimental Ge−O bond length in bulk Germania (1.74 Å)[30] and only 1.08% smaller than the value calculated for the Ge−O bond length (1.85 Å) corresponding to Ge^+.[28] Because the increased partial atomic charge on the noncompletely oxidized Ge atom can lead to a slight constriction of the Ge−O bond, there is a close relationship between Ge−O bond distance and Ge oxidation state: a higher oxidation state results in a decreased Ge−O bond length. Therefore, the oxidation state of oxidized Ge in configuration I should be a little higher than that of Ge^+. The bond length between Ge_3 and Ti_{12} atoms is ∼2.70 Å (listed in Table 9), which is very close (2.17% lower) to the experimental Ti−Ge bond length in bulk TiGeSb (2.76 Å)[31] and equal to the computed value in the bulk $Ti_3Si_{0.5}Ge_{0.5}C_2$.[32] Consequently, the state of Ge_3 atom in configuration I could be regarded as typical GeTi.

Let us now compare these computed charge transfers with Ge 3d core level photoemission measurements. The spectrum shown in Figure 11 has been obtained by depositing a small amount of Ge on a STO(001) surface previously strongly reconstructed by thermal annealing. The Ge 3d core level presents three components (each of them exhibits a spin−orbit splitting of 0.58 eV), which can be related to Ge bulk, GeO_x suboxide, and GeTi alloy. The GeTi component is shifted by 0.3 eV from the Ge component toward lower binding energy, whereas the GeO_x suboxide is shifted by 1.2 eV toward higher binding energy. Here again this proportionality between charge transfers and photoemission core level shifts is a good indicator of the pertinence of our model: first for the description of the initial STO surface and second for the Ge growth on it. Our calculated charge transfers (−0.15|e|, 0.58|e|) are proportional to the observed core-level shifts (−0.3 eV, 1.2 eV). Note that a GeO_x core level shift of 1.2 eV is in between the core level shifts of 0.85 and 1.70 eV expected for Ge^+ and Ge^{2+}[33,34] in Ge oxidation. This is not surprising because Ti−O−Ge bonds are concerned instead of only Ge−O−Ge, as already mentioned by Poutois et al. in ref 28 in the Ge/HfO_2 case. The consistency between the present calculation result and the experimental result of Ge 3d core level suggests that our optimized Ge (111) plane model can be regarded as a reasonable and realistic initial structure for Ge [111] direction growth on STO(001) surface.

dx.doi.org/10.1021/jp205074w |J. Phys. Chem. C XXXX, XXX, 000–000

4. CONCLUSIONS

In summary, we studied the Ge adsorption and heteroepitaxial growth on the $SrTiO_3$ (001) 2 × 1 DL TiO_2 surface via the first principles calculations. Our calculation results demonstrated that the initial growth process of Ge(111) is strongly dependent on the STO surface reconstruction. The results obtained in the present study can be summarized as follows.

(1) We first fully relaxed the STO (001) 2 × 1 DL TiO_2 surface and then computed its electronic structure. We make sure that it is reliable for the study by comparing the recorded soft-X-ray experiments of the annealed STO (001) surface with our results. Our calculations show that for this surface the Ti−O bond covalency increases while the Ti positive charge is decreased, leading to an enhanced attractivity of surface oxygen atoms (O_{13} and O_{14}).

(2) The germanium atom adsorption on STO (001) 2 × 1 DL TiO_2 surface is studied. Four kinds (B_{34}, B_{14}, TO_2, and H) of stable adsorption configurations are confirmed. By comparing their adsorption energies, we show that B_{34} configuration, which consists of O_{13} and O_{14}, is the most favorable one. Moreover, the minimum-energy paths of Ge atom surface migrations between different sites are achieved by studying approximate 2D potential energy surface and diffusion energy barriers. The potential energy surface shows that all energy minimums are located around the surface oxygen atoms O_{13} and O_{14}, and the diffusions from B_{14}, TO_2, and H sites to B_{34} site are very easy with energy barriers <0.45 eV. These results reveal that B_{34} has the highest probability to be formed on the STO (001) 2 × 1 DL TiO_2 surface at the ordinary germanium growth temperature. Consequently, the adsorbed Ge on this site will act as a nucleation center in the continuous process.

(3) Studying further Ge adsorption, we here found the most probable Ge(111)/STO(001) interface. The computed interface characteristic is shown to be in good agreement with experimental results obtained from a treatment of the grown Ge layer. Detailed structure parameters of the Ge(111)/STO(001) interface show that the high-quality Ge (111)-oriented film can be quickly produced on STO(001) surface. Because the surface floating oxygen atom (O_{14}) existence is a key point for the further (111) orientation of the Ge tetrahedrons on the STO surface, we suggest that Ge growth should be done in lower temperature condition to preserve the reconstruction integrity.

■ ACKNOWLEDGMENT

We acknowledge financial support from French ANR project COMPHETI, grant no. ANR-09-NANO-013-01. We also thank Northwestern Polytechnical University High Performance Computing Center for allocation of computing time on their machines.

■ REFERENCES

(1) Eisenbeiser, K.; Emrick, R.; Drropad, R.; Yu, Z.; Finder, J.; Rockwell, S.; Holmes, J.; Overgaard, C.; Ooms, W. *IEEE Electron Device Lett.* **2002**, *23*, 300.

(2) Seo, J. W.; Dieker, C.; Tapponier, A.; Marchiori, C.; Sousa, M.; Locquet, J.-P.; Fompeyrine, J.; Ipsas, A.; Rossel, C.; Panayiotatos, Y.; Sotiropoulos, A.; Dimoulas, A. *Microelectron. Eng.* **2007**, *84*, 2328.

(3) Giussani, A.; Rodenbach, P.; Zaumseil, P.; Dabrowski, J.; Kurps, R.; Weidner, G.; Schroeder, T. *J. Appl. Phys.* **2009**, *105*, 033512.

(4) Saint-Girons, G.; Cheng, J.; Regreny, P.; Largeau, L.; Patriarche, G.; Hollinger, G. *Phys. Rev. B* **2009**, *80*, 155308.

(5) Saint-Girons, G.; Regreny, P.; Largeau, L.; Patriarche, G.; Hollinger, G. *Appl. Phys. Lett.* **2007**, *91*, 241912.

(6) Merckling, C.; Delhaye, G.; El-Kazzi, M.; Gaillard, S.; Rozier, Y.; Rapenne, L.; Chenevier, B.; Marty, O.; Saint-Girons, G.; Gendry, M.; Robach, Y.; Hollinger, G. *Microelectron. Reliab.* **2007**, *47*, 540.

(7) Delhaye, G.; Merckling, C.; El-Kazzi, M.; Saint-Girons, G.; Gendry, M.; Robach, Y.; Hollinger, G.; Largeau, L.; Patriarche, G. J. *Appl. Phys.* **2006**, *100*, 124109.

(8) Cheng, J.; Aviles, T.; El Akra, A.; Bru-Chevallier, C.; Largeau, L.; Patriarche, G.; Regreny, P.; Benamrouche, A.; Robach, Y.; Hollinger, G.; Saint-Girons, G. *Appl. Phys. Lett.* **2009**, *95*, 232116.

(9) Cheng, J.; Regreny, P.; Largeau, L.; Patriarche, G.; Mauguin, O.; Naji, K.; Hollinger, G.; Saint-Girons, G. J. *Cryst. Growth* **2009**, *311*, 1042.

(10) El-Kazzi, M.; Gobaut, B.; Penuelas, J.; Grenet, G.; Silly, M.; Sirotti, F.; Saint-Girons, G. *Internal Report on Experiments Realized at TEMPO Soft X-rays Beamline at the French Synchrotron Radiation Source SOLEIL*; SOLEIL proposal no. 20090370; 2010.

(11) Wei, W.; Dai, Y.; Guo, M.; Zhu, Y.; Huang, B. *J. Phys. Chem. C* **2010**, *114*, 10917.

(12) Wei, W.; Dai, Y.; Guo, M.; Niu, C.; Huang, B. *Surf. Sci.* **2011**, *605*, 1331.

(13) Wei, W.; Dai, Y.; Lai, K.; Guo, M.; Huang, B. *Chem. Phys. Lett.* **2011**, *510*, 104.

(14) Wei, W.; Dai, Y.; Guo, M.; Huang, B. *Appl. Surf. Sci.* **2011**, *257*, 6607.

(15) Erdman, N.; Poeppelmeier, K. R.; Asta, M.; Warschkow, O.; Ellis, D. E.; Marks, L. D. *Nature* **2002**, *419*, 55.

(16) Heifets, E.; Piskunov, S.; Kotomin, E. A.; Zhukovskii, Y. F.; Ellis, D. E. *Phys. Rev. B* **2007**, *75*, 115417.

(17) Piskunov, S.; Heifets, E.; Eglitis, R. I.; Borstel, G. *Comput. Mater. Sci.* **2004**, *29*, 165.

(18) McSkimin, H. J. *J. Appl. Phys.* **1953**, *24*, 988. **1964**, *35*, 3312.

(19) Segall, M. D.; Lindan, P. J. D.; Probert, M. J. C.; Pickard, J.; Hasnip, P. J.; Clark, S. J.; Payne, M. C. *J. Phys.: Condens. Matter* **2002**, *14*, 2717.

(20) Perdew, J. P.; Burke, K.; Ernzerhof, M. *Phys. Rev. Lett.* **1996**, *77*, 3865.

(21) Monkhorst, H. J.; Pack, J. D. *Phys. Rev. B* **1976**, *13*, 5188.

(22) Tang, W.; Sanville, E.; Henkelman, G. *J. Phys.: Condens. Matter* **2009**, *21*, 084204.

(23) Bader, R. *Atoms in Molecules: A Quantum Theory*; Oxford University Press: New York, 1990.

(24) Segall, M. D.; Shah, R.; Pickard, C. J.; Payne, M. C. *Phys. Rev. B* **1996**, *54*, 16317.

(25) Iles, N.; Finocchi, F.; Khodja, K. D. *J. Phys.: Condens. Matter* **2010**, *22*, 305001.

(26) Piskunov, S.; Kotomin, E. A.; Heifets, E.; Maier, J.; Eglitis, R. I.; Borstel, G. *Surf. Sci.* **2005**, *575*, 75.

(27) Jiang, Z.; Zhang, W.; Jin, L.; Yang, X.; Xu, F.; Zhu, J.; Huang, W. *J. Phys. Chem. C* **2007**, *111*, 12434.

(28) Pourtois, G.; Houssa, M.; Delabie, A.; Conard, T.; Caymax, M.; Meuris, M.; Heyns, M. M. *Appl. Phys. Lett.* **2008**, *92*, 032105.

(29) Govind, N.; Petersen, M.; Fitzgerald, G.; King-Smith, D.; Andzelm, J. *J. Comput. Mater. Sci.* **2003**, *28*, 250.

(30) Wright, A. C.; Etherington, G.; Desa, J. A. E.; Sinclair, R. N.; Connell, G. A. N.; Mikkelsen, J. C. *J. Non-Cryst. Solids* **1982**, *49*, 63.

(31) Lam, R.; Mar, A. *Acta Crystallogr.* **2009**, *E65*, i68.

(32) Orellana, W.; Gutirrez, G.; Menndez-Proupin, E.; Rogan, J.; Garcia, G.; Manoun, B.; Saxena, S. J. *Phys. Chem. Solids* **2006**, *67*, 2149.

(33) Schmeisser, D.; Schnell, R. D.; Bogen, A.; Himpsel, F. J.; Roeger, D.; Landgren, G.; Morar, J. F. *Surf. Sci.* **1986**, *172*, 455.

(34) Renault, O.; Fourdrinier, L.; Martinez, E.; Clavelier, L.; Leroyer, C.; Barrett, N.; Crotti, C. *Appl. Phys. Lett.* **2007**, *90*, 052112.